

# Evidence for a non-zero $\Lambda$ and a low matter density from a combined analysis of the 2dF Galaxy Redshift Survey and Cosmic Microwave Background Anisotropies

G. Efstathiou<sup>1,2</sup>, Stephen Moody<sup>1</sup>, John A. Peacock<sup>3</sup>, Will J. Percival<sup>3</sup>, Carlton Baugh<sup>4</sup>, Joss Bland-Hawthorn<sup>5</sup>, Terry Bridges<sup>5</sup>, Russell Cannon<sup>5</sup>, Shaun Cole<sup>4</sup>, Matthew Colless<sup>6</sup>, Chris Collins<sup>7</sup>, Warrick Couch<sup>8</sup>, Gavin Dalton<sup>9</sup>, Roberto De Propis<sup>8</sup>, Simon P. Driver<sup>10</sup>, Richard S. Ellis<sup>11</sup>, Carlos S. Frenk<sup>4</sup>, Karl Glazebrook<sup>12</sup>, Carole Jackson<sup>6</sup>, Ofer Lahav<sup>1</sup>, Ian Lewis<sup>5</sup>, Stuart Lumsden<sup>13</sup>, Steve Maddox<sup>14</sup>, Peder Norberg<sup>4</sup>, Bruce A. Peterson<sup>6</sup>, Will Sutherland<sup>3</sup>, Keith Taylor<sup>11</sup> (The 2dFGRS Team)

1. *Institute of Astronomy, Madingley Road, Cambridge CB3 0HA, UK.*
2. *Theoretical Astrophysics, Caltech, Pasadena, CA 91125, USA.*
3. *Institute for Astronomy, University of Edinburgh, Royal Observatory, Blackford Hill, Edinburgh, EH9 3HJ, UK.*
4. *Department of Physics, University of Durham, South Road, Durham DH1 3LE, UK.*
5. *Anglo-Australian Observatory, P.O. Box 296, Epping, NSW 2121, Australia.*
6. *Research School of Astronomy and Astrophysics, The Australian National University, Weston Creek, ACT 2611, Australia*
7. *Astrophysics Research Institute, Liverpool John Moores University, Twelve Quays House, Birkenhead, L14 1LD, UK*
8. *Department of Astrophysics, University of New South Wales, Sydney, NSW 2052, Australia.*
9. *Astrophysics, Nuclear and Astrophysics Laboratory, University of Oxford, Keble Road, Oxford OX1 3RH, UK.*
10. *School of Physics and Astronomy, University of St Andrews, North Haugh, St Andrews, Fife, KY6 9SS, UK.*
11. *Department of Astronomy, Caltech, Pasadena, CA 91125, USA.*
12. *Department of Physics and Astronomy, Johns Hopkins University, Baltimore, MD 21218-2686, USA.*
13. *Department of Physics, University of Leeds, Woodhouse Lane, Leeds, LS2 9JT, UK.*
14. *School of Physics and Astronomy, University of Nottingham, Nottingham, NG7 2RD, UK.*

23 October 2018

## ABSTRACT

We perform a joint likelihood analysis of the power spectra of the 2dF Galaxy Redshift Survey (2dFGRS) and the cosmic microwave background (CMB) anisotropies under the assumptions that the initial fluctuations were adiabatic, Gaussian and well described by power laws with scalar and tensor indices of  $n_s$  and  $n_t$ . On its own, the 2dFGRS sets tight limits on the parameter combination  $\Omega_m h^*$ , but relatively weak limits on the fraction of the cosmic matter density in baryons  $\Omega_b/\Omega_m$ . The CMB anisotropy data alone set poor constraints on the cosmological constant and Hubble constant because of a ‘geometrical degeneracy’ among parameters. Furthermore, if tensor modes are allowed, the CMB data allow a wide range of values for the physical densities in baryons and cold dark matter ( $\omega_b = \Omega_b h^2$  and  $\omega_c = \Omega_c h^2$ ). Combining the CMB and 2dFGRS data sets helps to break both the geometrical and tensor mode degeneracies. The values of the parameters derived here are consistent with the predictions of the simplest models of inflation, with the baryon density derived from primordial nucleosynthesis and with direct measurements of the Hubble parameter. In particular, we find strong evidence for a positive cosmological constant with a  $\pm 2\sigma$  range of  $0.65 < \Omega_\Lambda < 0.85$ , completely independently of constraints on  $\Omega_\Lambda$  derived from Type Ia supernovae.

**Key words:** Galaxy clustering, large-scale structure, cosmic microwave background-cosmology: miscellaneous.

\* Here  $h$  is Hubble’s constant  $H_0$  in units of  $100\text{kms}^{-1}\text{Mpc}^{-1}$ .

The cosmic densities in baryons, cold dark matter and vacuum

## 1 INTRODUCTION

Until recently, cosmology was a subject starved of data, with poor or non-existent constraints on fundamental quantities such as the curvature of the Universe, the power spectrum of density irregularities, and the cosmic densities in baryons, cold dark matter and vacuum energy. The situation has changed dramatically over the last few years. Following the discovery of the CMB anisotropies (Smoot et al. 1992) it was realized that many of the fundamental parameters of our Universe could be determined via accurate, high resolution measurements of the CMB (*e.g.* Bond et al. 1994, Jungman et al. 1996). This has now become a reality through a number of exquisite ground based and balloon experiments (see Halverson et al. 2001; Lee et al. 2001; Netterfield et al. 2001). Constraints on cosmological parameters derived from these experiments are described in several recent papers (de Bernadis et al. 2001; Pryke et al. 2001; Stompor et al. 2001; Wang, Tegmark & Zaldarriaga 2001).

Significant advances have also been made in surveying large scale structure in the Universe. The development of wide-field correctors and multi-fibre spectroscopy means that it is now possible to measure redshifts of hundreds of thousands of galaxies. Two such redshift surveys are underway. The 2dF Galaxy Redshift Survey (2dFGRS) utilises the 2dF instrument at the Anglo-Australian Telescope and is based on a revised version of the APM Galaxy Survey (Maddox et al. 1990) limited at  $b_J = 19.45$ . Redshifts have now been measured for over 175 000 galaxies (see Colless et al. 2001, for a description of this survey). The Sloan Digital Sky Survey (SDSS, York et al. 2000) is a CCD imaging and spectroscopic survey that aims to measure redshifts for a sample of 900 000 galaxies. An analysis of the galaxy power spectrum from the 2dFGRS is described by Percival et al. (2001, hereafter P01). First results on galaxy clustering from a subsample of the SDSS are presented by Zehavi et al. (2001).

In addition, a number of other investigations have greatly improved the accuracy of various cosmological parameters. For example, surveys of high redshift Type Ia supernovae have revealed tantalizing evidence for an accelerating Universe (Perlmutter et al. 1999, Riess et al. 1999); the HST Hubble key project has concluded that  $H_0 = 72 \pm 8 \text{ km s}^{-1} \text{ Mpc}^{-1}$  (Freedman et al. 2001); primordial nucleosynthesis and deuterium abundance measurements from quasar absorption lines imply a baryon density  $\omega_b = 0.020 \pm 0.002$  (Burles & Tytler 1998ab; Burles, Nollett & Turner 2001). With these and many other ambitious projects at various stages of development (*e.g.* weak shear lensing surveys, CMB interferometers, CMB polarization experiments, the MAP, Planck and SNAP satellites<sup>†</sup>) it is clear that the era of quantitative cosmology has arrived.

In this paper, we perform a combined likelihood analysis of the CMB anisotropy data and of the 2dFGRS galaxy power spectrum measured by P01. We assume that the initial fluctuations were Gaussian, adiabatic and described by

energy are denoted by  $\Omega_b$ ,  $\Omega_c$  and  $\Omega_\Lambda$ . The total matter density is  $\Omega_m = \Omega_b + \Omega_c$  and the curvature is fixed by  $\Omega_k = 1 - \Omega_m - \Omega_\Lambda$ .

<sup>†</sup> Descriptions of these satellites can be found on the following web pages: <http://snap.lbl.gov/>, <http://map.gsfc.nasa.gov/>, <http://astro.estec.esa.nl/SA-general/Projects/Planck>.

power-law fluctuation spectra. Matter is assumed to consist of baryons and cold dark matter (CDM) and neutrinos are assumed to have negligible rest masses. We allow tensor and scalar modes and place no constraints on their respective spectral indices and relative amplitudes. Almost all previous analyses of the CMB anisotropies have neglected tensor modes. However, including tensor modes introduces a major new degeneracy (referred to as the *tensor degeneracy* in this paper) that significantly widens the range of allowed parameters (see Efstathiou & Bond 1999, Wang et al. 2001, Efstathiou 2001). The tensor degeneracy can be broken by invoking additional data sets. Wang et al. 2001 combine the CMB data with measurements of the galaxy power spectrum from the IRAS PSCz survey (Hamilton, Tegmark & Padmanabhan 2000), estimates of the power spectrum on small scales from observations of the Ly $\alpha$  forest (Croft et al. 2001) and limits on the Hubble constant from HST Hubble Key Project. Here we investigate how the major parameter degeneracies can be broken by combining the CMB data with the 2dFGRS power spectrum. The 2dFGRS power spectrum is based on a large survey, with well controlled errors, and as demonstrated by P01 already sets interesting limits on the matter content of the Universe. Our expectation (see Efstathiou 2001) is that a joint analysis of the CMB and 2dFGRS will produce accurate estimates of the baryonic and matter densities of the Universe and set useful limits on a cosmological constant. This expectation is borne out by the results described in the rest of this paper.

## 2 LIKELIHOOD ANALYSIS

### 2.1 Analysis of the 2dFGRS power spectrum

We use the estimates of the galaxy power spectrum and associated covariance matrix computed by P01. As in P01, we fit these estimates to theoretical models of the linear matter power spectrum of CDM models using the fitting formulae of Eisenstein & Hu (1998). The fits are restricted to the wavenumber range  $0.02 < k/(h \text{ Mpc}^{-1}) < 0.15$ . Redshift-space distortions (see Peacock et al. 2001) and non-linear evolution of the power spectrum have negligible effect on the shape of the power spectrum at these wavenumbers. We will assume that the galaxy power spectrum within this wavenumber range is directly proportional to the linear matter power spectrum. This is a key assumption in the analysis presented in this paper. The lower wavenumber limit is imposed (conservatively) to reduce the sensitivity of the analysis to fits to the redshift distribution of galaxies, which are computed independently for different zones of the survey. Since the 2dFGRS has a complex geometry, the theoretical power spectra must be convolved with the spherical average over wavenumber of the survey ‘window function’. These convolved theoretical estimates are used together with the spherically averaged estimates of the power spectrum of the data and the covariance matrix (computed from Gaussian realizations of the 2dFGRS) to form a likelihood function. We refer the reader to P01 for a full discussion of each of these steps in the analysis.

In general, the linear power spectrum with wavenumber measured in inverse Mpc depends on the baryonic and CDM physical densities ( $\omega_b$  and  $\omega_c$ ), the scalar spectral index  $n_s$  and an overall amplitude  $A$  (the amplitude is treated

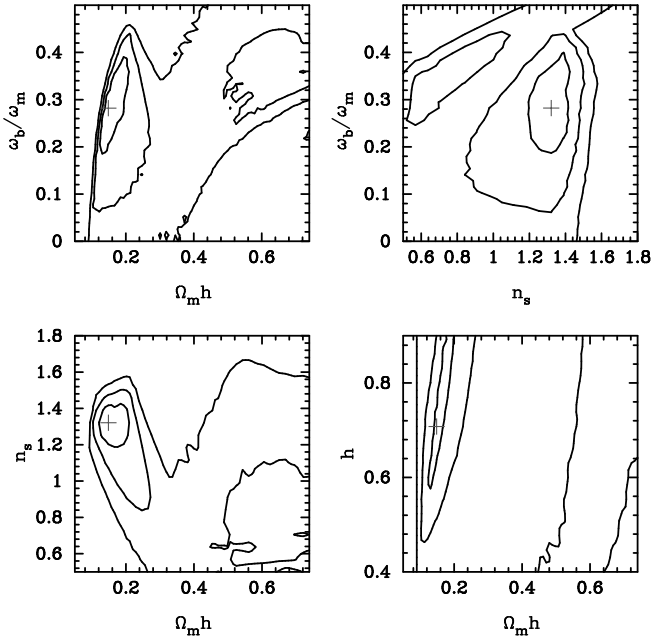


**Figure 1.** Contours (1, 2 and  $3\sigma$ ) of the pseudo-marginalized likelihood functions (see text for details) for various pairs of parameters computed by fitting to the galaxy power spectrum of the 2dFGRS. These contours correspond to changes in the likelihood of  $2\Delta\ln(\mathcal{L})$  of 2.3, 6.0 and 9.2. The crosses show the position of maximum likelihood.

as an ‘ignorable’ parameter in this paper and so its precise definition is unimportant). However since we use redshift to measure distances, the wavenumber of the observations scales as  $h \text{ Mpc}^{-1}$ . The comparison of theory with observations therefore requires the introduction of the parameter  $h$ . In fact, the set of variables  $A$ ,  $n_s$ ,  $\Omega_m h$ ,  $\omega_b/\omega_m$  and  $h$  are natural variables for an analysis of large-scale structure: the combination  $\Omega_m h$  defines the overall shape of the CDM transfer function (and for negligible baryon density is sometimes denoted by the shape parameter  $\Gamma$ ), while the ratio  $\omega_b/\omega_m$  determines the amplitude of baryonic oscillatory features in the transfer function (Eisenstein & Hu 1998; Meiksin, Peacock & White 1999).

Fig. 1 shows various two-dimensional projections of the ‘pseudo-marginalized’ 2dFGRS likelihood function. When using a large number of parameters (as in the CMB and CMB+2dFGRS analyses described in the next two subsections), it is impractical to compute marginalized likelihood contours by numerically integrating over the likelihood distribution. Instead, a ‘pseudo-marginalized’ likelihood function in  $p$  out of  $M$  parameters is computed by setting the remaining  $M - p$  parameters at the values which maximise the likelihood. For a multivariate Gaussian distribution, this is equivalent to integrating over the  $M - p$  parameters assuming uniform prior distributions (see Tegmark, Zaldarriaga & Hamilton 2001). However, the actual likelihood distributions are not exactly Gaussian (as is evident from the asymmetrical contours in Figs 1 and 3) and so confidence limits assigned to pseudo-marginalized distributions are approximate. The contours in the  $(\omega_b/\omega_m, \Omega_m h)$  plane can be compared with Fig. 5 of P01 where the spectral index was as-

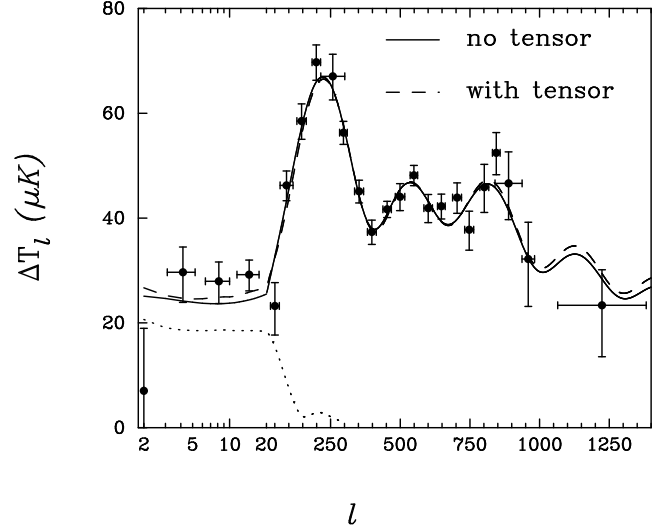


**Figure 2.** The points show band-averaged observational estimates of the CMB power spectrum from Wang et al. (2001) together with  $\pm 1\sigma$  errors. The lines show the CMB power spectra for the adiabatic fiducial inflationary models that provide the best fit to the CMB and 2dFGRS power spectra. The parameters of these model are listed in Table 1. The solid line shows the best fit without a tensor component (fit B). The dashed line shows the best fit (fit C) including a tensor component (shown by the dotted line).

sumed to be scale invariant. Relaxing the constraint on the spectral index clearly widens the allowed range of  $\omega_b/\omega_m$ , but the data still place a tight constraint on the ‘shape’ parameter  $\Omega_m h$ . As we will see below, the constraints on  $\Omega_m h$  and  $n_s$  prove particularly important in breaking degeneracies among parameters inherent in the analysis of CMB data.

## 2.2 Analysis of the CMB anisotropies

The likelihood analysis presented here uses the compilation of band power estimates  $\Delta T_B^2$  and their covariance matrix  $C_{BB'}$  (including a model for calibration and beam errors) computed by Wang et al. (2001) from 105 CMB anisotropy measurements. Each band power estimate is related to the power spectrum  $C_\ell$  of the CMB anisotropies by

$$\Delta T_B^2 = \frac{T_0^2}{2\pi} \sum_{\ell} \ell(\ell+1) C_{\ell} W_B(\ell) \quad (1)$$

where  $W_B$  is the window function for each band power computed by Wang et al. These band-power estimates are plotted in Fig. 2.

The likelihood analysis of the CMB data uses nine parameters. These are:  $\omega_b$  and  $\omega_c$ ;  $\Omega_{\Lambda}$  and  $\Omega_k$ ; the scalar and tensor spectral indices  $n_s$  and  $n_t$ ; the optical depth to Thomson scattering  $\tau_{opt}$ , assuming that the inter-galactic medium was abruptly reionized some time after recombination; the amplitude  $Q^2$  of the scalar component and the ratio of  $\bar{r}$  of the tensor to scalar amplitudes. Note that definitions of the scalar and tensor amplitudes differ from paper to paper.

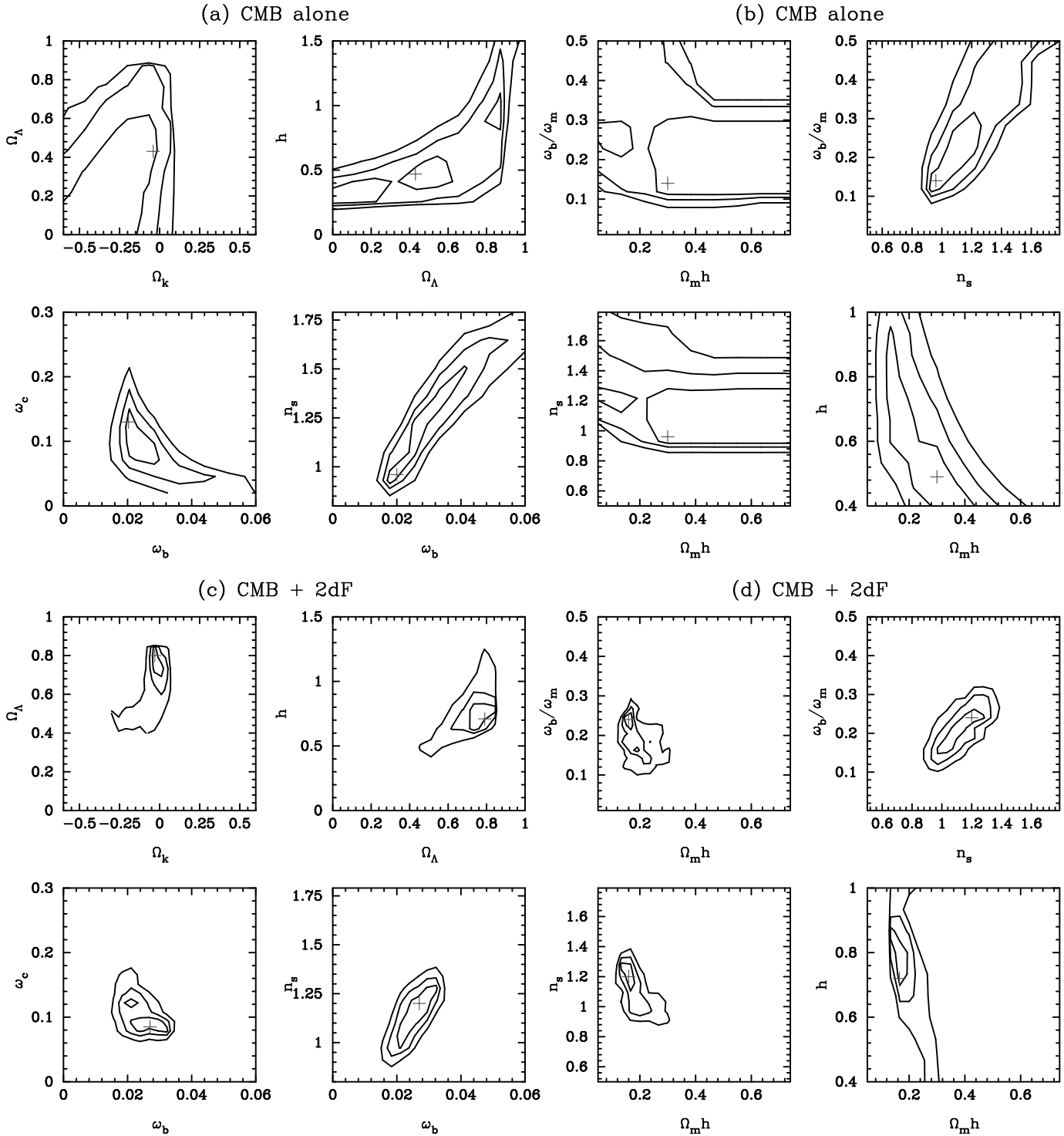


**Figure 3.** Results of the nine parameter likelihood analysis. Figs 3a and 3b show approximate 1, 2 and 3 $\sigma$  likelihood contours for various parameter pair combinations computed from an analysis of the CMB data alone. Figs 3a use variables natural to the CMB analysis and illustrate the geometrical and tensor degeneracies. Figs 3b use the variables natural to the analysis of the galaxy power spectrum (as used in Fig. 1). Figs 3c and 3d show the likelihood contours of CMB and 2dFGRS data combined. The crosses in each panel show the position of the maximum likelihood.

Here we scale the scalar and tensor spectra so that

$$\frac{1}{4\pi} \sum_{\ell=2}^{1000} (2\ell+1) \hat{C}_\ell^S = (4 \times 10^{-5})^2, \quad (2a)$$

$$\frac{1}{4\pi} \sum_{\ell=2}^{50} (2\ell+1) \hat{C}_\ell^T = (2 \times 10^{-5})^2, \quad (2b)$$

and fit to the data by scaling with the parameters  $Q$  and  $\bar{\tau}$ ,  $C_\ell = C_\ell^S + C_\ell^T = Q^2(\hat{C}_\ell^S + \bar{\tau}\hat{C}_\ell^T)$ . The numbers in equation (2) were chosen so that models with  $Q$  of approximately unity match the data points plotted in Fig. 2 and models with  $\bar{\tau} \approx 1$  have scalar and tensor modes of comparable amplitude. We normalize the spectra in this way to reduce the sensitivity of the normalization parameters to other parameters that affect the low order multipole moments (*e.g.*  $\Omega_\Lambda$  and  $\Omega_k$ ) and to decouple  $Q$  from the optical depth parameter  $\tau_{opt}$ . This method of normalizing helps to stabilize searches for global maxima of the likelihood functions. For our best fit models of Table 1 below we list values of the more commonly used parameter  $r_{10} \equiv C_{10}^T/C_{10}^S$  in addition to  $\bar{\tau}$ . In simple models of inflation, the parameters  $r_{10}$  (or  $\bar{\tau}$ ),  $n_s$  and  $n_t$  are related to each other (see *e.g.* Hoffman & Turner 2001 for a recent discussion). The relations are model dependent, however, and can be violated in multi-field inflation models and in superstring inspired models such as the pre-big bang (Buonanno, Damour & Veneziano 1999) and ekpyrotic scenarios (Khoury, Ovrut, Steinhardt & Turok 2001). We therefore assume no relations between  $r_{10}$ ,  $n_s$  and  $n_t$  in this paper.

Results from the likelihood analysis of the CMB data are illustrated in Fig. 3. Almost all of the variance of the parameters used in this analysis, with the exception of  $Q$ , comes from two major degeneracies (see Efstathiou 2001 for a detailed discussion). These two degeneracies are illustrated by the likelihood contours plotted in Fig. 3a. The top two panels illustrate the ‘geometrical’ degeneracy. This degeneracy arises because models with identical matter content, primordial power spectra and angular diameter distance to the last scattering surface produce almost identical CMB power spectra. This leads to a strong degeneracy between  $\Omega_\Lambda$  and  $\Omega_k$ , which is broken only for extreme values of  $\Omega_\Lambda$  by the integrated Sachs-Wolfe effect which modifies the shape of the CMB power spectrum at low multipoles (see Efstathiou & Bond 1999). Since the Hubble constant is fixed by the constraint equation,

$$h = \frac{(\omega_b + \omega_c)^{1/2}}{(1 - \Omega_k - \Omega_\Lambda)^{1/2}}, \quad (3)$$

it is almost unconstrained by the CMB data.

The lower two panels in Fig. 3a show the constraints on the parameter combinations  $\omega_c - \omega_b$  and  $n_s - \omega_b$ . These panels illustrate the tensor degeneracy: including a tensor component significantly broadens the allowed ranges of parameters. For example, values of  $\omega_b$  that are more than twice the value favoured from primordial nucleosynthesis are allowed by the CMB data (Efstathiou 2001).

Fig. 3b shows likelihood contours using the CMB data alone, but computed with the natural variables of the galaxy power spectrum analysis as in Fig. 1. The parameter combination  $\Omega_m h$  that essentially fixes the shape of the matter power spectrum is extremely unnatural for an analysis of the

CMB anisotropies. Since  $\Omega_m h \equiv (\omega_b + \omega_c)/h$ , the indeterminacy in  $h$  arising from the geometrical degeneracy smears the likelihoods along the direction of  $\Omega_m h$ . The wide range of allowed values of  $\omega_b/\omega_m$  and the tight correlation with  $n_s$  is a consequence of the tensor degeneracy.

### 2.3 Combining the CMB and 2dFGRS likelihoods

Fig. 3b is interesting because it shows that the CMB likelihoods in three of these plots are complementary to those of the 2dFGRS analysis ( $\omega_b/\omega_m - \Omega_m h$ ,  $n_s - \Omega_m h$ ,  $\omega_b/\omega_m - n_s$ ). The addition of the 2dFGRS constraints breaks both the geometrical and tensor degeneracies, resulting in strong constraints on  $\omega_b$ ,  $\omega_c$ ,  $\Omega_\Lambda$  and  $h$ . The way that this works is evident from Figs 1 and 3b: the constraints on  $n_s$  from the 2dFGRS help to break the tensor degeneracy by excluding high values of  $\omega_b$  and low values of  $\omega_c$ . The resulting values of  $\omega_b$  and  $\omega_c$  fix the Hubble radius at the time that matter and radiation have equal density, which in turn largely fixes the shape of the CDM transfer function in physical Mpc. Comparing with the power spectrum of the 2dFGRS in  $h^{-1}$ Mpc constrains the Hubble constant, thus breaking the geometrical degeneracy.

The lower panels in Fig. 3 show the results of combining the CMB and 2dFGRS likelihoods. The results are striking, showing a significant tightening of the constraints in each plot. Table 1 lists parameters corresponding to maximum likelihood fits to the data and the approximate  $\pm 2\sigma$  ranges of each parameter. The second column lists the maximum likelihood fit to the CMB alone (fit A). The parameters of this fit are identical whether or not a tensor component is included. The third and fourth columns (fits B and C) list the maximum likelihood fits to the CMB and 2dFGRS data excluding and including a tensor mode. The fifth column (fit D) adds the constraint from big-bang nucleosynthesis (BBN) of a Gaussian distribution for  $\omega_b$  centred at  $\omega_b = 0.020$  with a dispersion of  $\Delta\omega_b = 0.001$  (Burles et al. 2001).

The parameters of fit B, which provides a perfectly acceptable fit to the data, are very close to those of the standard ‘concordance’ cosmology (*e.g.* Bahcall et al. 1999). In particular, the baryon density is compatible with the primordial nucleosynthesis value, and the Hubble and cosmological constants are compatible with more direct observational estimates. The CMB power spectrum for this solution is plotted as the solid line in Fig. 2 and the linear matter power spectrum is plotted together with the 2dFGRS data points in Fig. 4. Both curves provide acceptable fits to the data. Fit B has a low baryon fraction of  $\omega_b/\omega_m = 0.15$ . As a consequence, the amplitudes of the baryonic features in the matter power spectrum are almost imperceptibly small (see Fig. 4).

Allowing a tensor component produces a slightly better fit to the data, but the parameters are less concordant with other observations (Fit C, Table 1). The CMB power spectrum for this model is plotted as the dashed line in Fig. 2. According to this solution, a significant part of the COBE anisotropies comes from a tensor component. The baryon density of fit C is  $\omega_b = 0.027$  and is well outside the range of values inferred from primordial nucleosynthesis. The matter power spectrum for this model is plotted as the dashed line in Fig. 4. This shows clearly what is happening with this solution. The apparent wiggles in the 2dFGRS power

**Table 1: Parameters values and errors**

	Fit A	Fit B	Fit C	Fit D	approximate $\pm 2\sigma$ parameter ranges		
	CMB alone + tensor	CMB+2dFGRS no tensor	CMB+2dFGRS + tensor	CMB+2dFGRS+BBN + tensor	Fit A CMB alone + tensor	Fit C CMB+2dFGRS + tensor	Fit D CMB+2dFGRS+BBN + tensor
$\omega_b$	0.020	0.021	0.027	0.020	0.016–0.045	0.018–0.034	0.018–0.022
$\omega_c$	0.13	0.12	0.085	0.10	0.03–0.18	0.07–0.13	0.08–0.13
$n_s$	0.96	1.00	1.20	1.04	0.89–1.49	0.95–1.31	0.95–1.16
$\Omega_k$	-0.04	0.001	-0.030	-0.013	-0.68–0.06	-0.05–0.04	-0.05–0.04
$\Omega_\Lambda$	0.43	0.71	0.80	0.73	< 0.88	0.65–0.85	0.65–0.80
$\tau_{opt}$	0	0	0	0	< 0.5	< 0.5	< 0.5
$n_t$		-	-0.10	0.13			
$\bar{\tau}$	0	-	0.60	0.20	< 0.98	< 0.87	< 0.82
$r_{10}$	0	-	1.24	0.26			
$\omega_b/\omega_m$	0.14	0.15	0.24	0.17	0.10–0.40	0.13–0.28	0.13–0.22
$\Omega_m h$		0.21	0.16	0.19		0.12–0.22	0.16–0.21
$h$		0.69	0.71	0.66		0.60–0.86	0.61–0.84

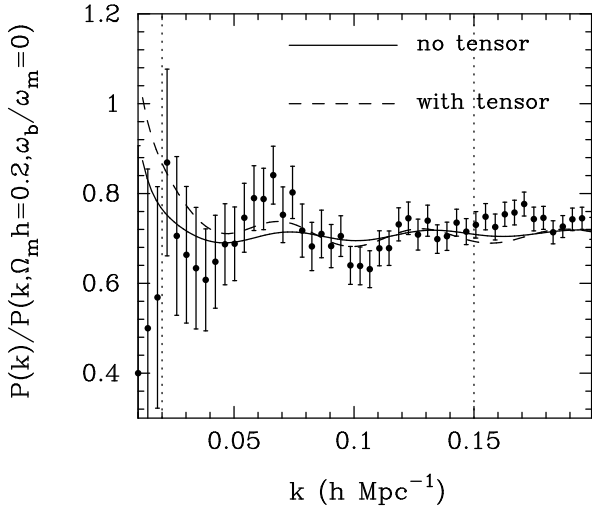


**Figure 4.** The points show the galaxy power spectrum of the 2dFGRS measured by P01 divided by the power spectrum of a scale-invariant CDM model with  $\omega_b = 0$ ,  $\Omega_m h = 0.2$ . The error bars are computed from the diagonal components of the covariance matrix. The lines show the linear matter power spectra of the maximum likelihood fits to the combined CMB and 2dFGRS power spectra after convolution with the spherically averaged window function of the survey. The solid line shows fit B from Table 1 (no tensor component). The dashed line shows fit C (including a tensor component).

spectrum pull the solution towards a high baryon fraction. However, to produce a good fit to the CMB anisotropies with a high baryon fraction, the tensor degeneracy of Fig. 3 requires high values of  $n_s$  and significant tensor anisotropies. The likelihood ratio of fits B and C is  $\mathcal{L}_B/\mathcal{L}_C = 0.34$  and so fit C is only marginally preferred over fit B. In two of the panels from Fig. 3c and d, the likelihood distributions have two peaks centred at the parameters of fits B and C. Adding the BBN constraint on  $\omega_b$  (fit D) selects one of these peaks with parameters close to those of fit B.

Fits B and C predict a lower normalization for the present day matter power spectrum than implied by the local abundance of rich clusters of galaxies. In a recent anal-

ysis of the number density distribution of rich clusters as a function of X-ray temperature, Pierpaoli, Scott and White (2001) deduce

$$\sigma_8 = (0.495_{-0.037}^{+0.034})\Omega_m^{-0.60}, \quad (4)$$

where  $\sigma_8$  is the rms fluctuation in the mass density distribution averaged in spheres of radius  $8h^{-1}\text{Mpc}$ . Fit B gives  $\sigma_8 = 0.72$  and fit C gives  $\sigma_8 = 0.61$ , whereas equation (4) implies  $\sigma_8 = 1.04$  and  $\sigma_8 = 1.20$  respectively. Most of the error in equation (4) comes from uncertainties in the cluster mass-X-ray temperature relation and it is not clear whether the quoted error reflects the true uncertainties. A number of effects could boost the best fitting values of  $\sigma_8$ , for example, a realistic value for  $\tau_{opt}$  or possible calibration errors in the CMB data might affect  $\sigma_8$  at the 10–20% level. Such effects may reconcile fit B with the cluster data, but are probably not large enough to explain the discrepancy with fit C. Furthermore, as we have discussed above, the discrepancy with the primordial nucleosynthesis value of  $\omega_b$  provides another reason to disfavour fit C.

### 3 DISCUSSION

The results of this paper are based on the key assumption that the galaxy power spectrum on large scales (wavenumbers  $k < 0.15h \text{ Mpc}^{-1}$ ) is proportional to the linear matter power spectrum. Under this assumption, we have shown that the galaxy power spectrum of the 2dFGRS can be used to partially break the two major parameter degeneracies inherent in the analysis of CMB anisotropies. The limits on the scalar spectral index from the 2dFGRS help to break the tensor degeneracy. The resulting constraints on the matter density provide a measure of a standard physical distance (the Hubble radius at the time that matter and radiation have equal density). This standard length constrains the Hubble constant and so breaks the geometrical degeneracy.

The resulting constraints are in remarkable agreement with the baryon density inferred from primordial nucleosynthesis (Burles and Tytler 1998ab), estimates of the Hubble constant from the HST Hubble key project (Freedman et al. 2001) and evidence for a non-zero cosmological constant from observations of distant Type Ia supernovae (Perlmutter et al. 1999; Riess et al. 1999). The best fit model excluding

a tensor component has parameters that are very close to those of the standard ‘concordance’ cosmology (Bahcall et al. 1999). However, the combined CMB+2dFGRS data provide weak upper limits on a tensor component (Table 1) and other solutions are possible which have a higher baryon density and baryon fraction. These solutions conflict with the limits on  $\omega_b$  from primordial nucleosynthesis and require a scalar spectral index  $n_s > 1$ . The model with high  $n_s$  and high  $\omega_b$  provides a somewhat closer match to the apparent ‘wiggles’ in the galaxy power spectrum at wavenumbers  $k \sim 0.08h \text{ Mpc}^{-1}$  and  $k \sim 0.12h \text{ Mpc}^{-1}$  than is achieved by the scalar only model (Fig. 4). Neither model fully matches the data points, however, and it is plausible that the apparent features are enhanced by the noise. New power spectrum data from the 2dFGRS and the SDSS will soon allow us to test this hypothesis. It is particularly encouraging that the combination of the 2dFGRS and CMB data yields strong evidence for a cosmological constant in the range  $0.65 \lesssim \Omega_\Lambda \lesssim 0.85$  based on completely different arguments to those applied to distant Type Ia supernovae. This significantly strengthens the case in favour of an accelerating universe.

**Acknowledgments:** GE thanks Caltech for the award of a Moore Scholarship. The CMB power spectra in this paper were computed using the CMBFAST code of Seljak & Zaldarriaga (1996).

## REFERENCES

- Bahcall N.A., Ostriker J.P., Perlmutter S., Steinhardt P.J., 1999, *Science*, 284, 1481.
- Bond J.R., Efstathiou G., Tegmark M., 1997, *MNRAS*, 291, L33.
- Bond J.R., Crittenden R., Davis R.L., Efstathiou G., Steinhardt P.J., 1994, *PRL*, 72, 13.
- Burles S., Tytler D., 1998a, *ApJ*, 499, 699.
- Buonanno, A., Damour T., Veneziano G., 1999, *Nucl. Phys. B.*, 543, 275.
- Burles S., Tytler D., 1998b, *ApJ*, 507, 732.
- Burles S., Nollett K.M., Turner M.S., 2001, *ApJL*. astro-ph/0010171.
- Colless M. et al., 2001, submitted to *MNRAS*. astro-ph/0106498.
- Croft R.A.C., Weinberg D.H., Bolte M., Burles S., Hernquist L., Katz K., Kirkman D., Tytler D., 2001, *ApJ*, in press. astro-ph/0012324.
- de Bernardis et al., 2001, astro-ph/0012324.
- Efstathiou G., Bond J.R., 1999, *MNRAS*, 304, 75.
- Efstathiou G., 2001, astro-ph/0109151.
- Eisenstein D.J., Hu W., 1998, *ApJ*, 496, 605.
- Freedman W.L. et al., 2001, *ApJ.*, 553, 47.
- Halverston N.W. et al. 2001, astro-ph/0104489.
- Hamilton A.J.S., Tegmark M., Padmanabhan N., 2000, *MNRAS*, 317, L23.
- Hoffman M.B., Turner M.S., 2001, *Phs. Rev. D.*, 64, 023506.
- Jungman, G., Kamionkowski M., Kosowsky A., Spergel D.N., 1996, *Phys. Rev. D.*, 54, 1332.
- Khoury J., Ovrut B.A., Steinhardt, P.J., Turok N., 2001, hep-th/0103239.
- Lee A.T. et al., 2001, astro-ph/0104459 .
- Maddox S.J., Efstathiou G., Sutherland W.J., Loveday J., 1990, *MNRAS*, 242, 43p.
- Meiksin A., Peacock J.A., White M., 1999, *MNRAS*, 304, 851.
- Netterfield C.B., et al. 2001, astro-ph/0104460.
- Peacock J.A. et al., 2001, *Nature*, 410, 169.
- Percival W.J. et al., 2001, *MNRAS*, in press. astro-ph/0105252.
- Perlmutter S. et al., 1999, *ApJ*, 517, 565.
- Pierpaoli E., Scott D., White M., 2001, *MNRAS*, 325, 77.
- Pryke C., Halverson N.W., Leitch E.M., Kovac J., Carlstrom J.E., Holzzapfel W.L., Dragovan M, submitted to *ApJ*, astro-ph/0104490.
- Riess A.G. et al., 1999, *AJ*, 117, 707.
- Seljak U., Zaldarriaga M., 1996, *ApJ*, 3469, 437.
- Smoot G.F. et al. 1992, *ApJ*, 396, L1.
- Stompor R. et al., submitted to *ApJL*, astro-ph/0106451.
- Tegmark M., Zaldarriaga M., Hamilton A.J.S., 2001, *Phys. Rev. D.*, 63, 043007.
- Wang X., Tegmark M., Zaldarriaga M., 2001, astro-ph/0105091.
- York D.G. et al., 2000, *AJ*, 120, 1579.
- Zaldarriaga, M., Spergel D.N., Seljak U., 1997 *ApJ*, 488, 1.
- Zehavi I. et al., 2001, astro-ph/0106476.